Biosensors and Bioelectronics 143 (2019) 111619

Contents lists available at ScienceDirect

Biosensors and Bioelectronics

journal homepage: www.elsevier.com/locate/bios

Ratiometric SERS biosensor for sensitive and reproducible detection of microRNA based on mismatched catalytic hairpin assembly

Jinyang Chen[a], Yan Wu[a,b,*], Cuicui Fu[a], Haiyan Cao[a], Xiaoping Tan[a], Wenbing Shi[a], Zhaoyang Wu[b]

[a] Chongqing Key Laboratory of Inorganic Special Functional Materials, College of Chemistry and Chemical Engineering, Yangtze Normal University, Fuling, Chongqing, 408100, China

[b] State Key Laboratory of Chemo/Biosensing and Chemometrics, College of Chemistry and Chemical Engineering, Hunan University, Changsha, 410082, China

ARTICLE INFO

Keywords:
Surface-enhanced Raman scattering
Catalytic hairpin assembly
microRNA
Ratiometric

ABSTRACT

MicroRNAs (miRNAs) serve as significant regulators in a variety of diseases and have been emerging as a class of promising biomarkers for early cancer diagnosis. Herein, an enzyme-free surface-enhanced Raman scattering (SERS) platform was proposed for sensitive and reliable detection of target miRNA-21 using a corrective internal standard (IS)-based ratiometric SERS probe coupled with mismatched catalytic hairpin assembly (CHA) amplification. The 4-aminothiophenol (4-ATP) was used as IS molecule and modified on the surface of silver nanoparticles decorated silicon wafer. In principle, the presence of miRNA-21 could cyclically trigger the allosteric effects of mismatched CHA amplification and the 3′-R6G labeled hairpin probe 1 (H1) was opened. Then, the hairpin probe 2 (H2) hybridized with H1 to form H1–H2 complex and the released miRNA-21 was free to participate in the next cycle of CHA reaction. Meanwhile, the H1–H2 complex could hybridize with the capture DNA on the SERS chip, making the Raman tag of R6G close to the surface of SERS substrate, and the intensity of SERS signal from R6G labels increase while that from 4-ATP remain relatively unchanged. Benefiting from outstanding performances of the ratiometric SERS strategy and enzyme-free CHA amplification system, this platform exhibits sensitivity toward miRNA-21 with a limit of detection of 3.5 fM and a broad dynamic range from 10 fM to 100 nM. More importantly, this proposed method presents an excellent reliable SERS analysis with the correction of IS. The developed strategy holds a potential alternative tool for miRNA detection in biomedical research and early clinical diagnosis.

1. Introduction

MicroRNAs (miRNAs) play significant roles in a diverse range of biological processes, including apoptosis, differentiation, developmental regulation, and cell proliferation, etc. (Bushati and Cohen, 2007; Dong et al., 2013). Recently, accumulative evidences have revealed that many diseases, such as cancers, genetic disorders, and neurological disorders are closely related with aberrant miRNA expression (Boon et al., 2013; Jeffrey, 2008; Lu et al., 2005). Thus, miRNAs are considered as promising biomarkers for early clinical diagnosis (Kosaka et al., 2010; Qiu et al., 2018). However, it remains a great challenge for miRNA detection owing to their short lengths, highly homologous sequences, vulnerable degradability, and relatively low expression levels in cells. Therefore, it is imperative to develop sensitive, specific and reliable miRNAs detection strategies for biomedical research and early clinical diagnosis.

Excellent review papers have summarized the main current achievements, challenges, and development of miRNA biosensors (D'Agata and Spoto, 2019; Kilic et al., 2018; Mohammadi et al., 2019). Moreover, a variety of current strategies have been proposed for miRNA detection, including electrochemical (Masud et al., 2019; Rafiee-Pour et al., 2016), colorimetric (Dong et al., 2018; Wu et al., 2016), fluorescent (Causa et al., 2015; Guk et al., 2019; Zhou et al., 2019b), electrochemiluminescent (Zhang et al., 2015a; Zhu and Ding, 2019), and surface-enhanced Raman spectroscopy (SERS) (Lee et al., 2018; Zhou et al., 2017). Currently, SERS strategy has attracted much attention in biological analysis (Cialla-May et al., 2017; Jayanthi et al., 2017). On the basis of its specific signal attainability, ultrasensitivity, rapidity, small sample volume requirement, and nondestructivity, SERS has been recognized as a promising strategy for miRNA detection (Lee et al.,

* Corresponding author. Chongqing Key Laboratory of Inorganic Special Functional Materials, College of Chemistry and Chemical Engineering, Yangtze Normal University, Fuling, Chongqing, 408100, China.
E-mail address: wyan2018@163.com (Y. Wu).

https://doi.org/10.1016/j.bios.2019.111619
Received 28 July 2019; Accepted 19 August 2019
Available online 22 August 2019

2019; Su et al., 2017). However, most of SERS miRNA strategies are focused on single response signal for determination (Driskell et al., 2008; He et al., 2017; Pang et al., 2019), which can be easily interrupted by the poorly reproducible and relative fluctuation SERS signal originated from the interference of working conditions and surroundings like laser power, focusing depth, and surface roughness, and even molecular structures, making it difficult to realize quantitative SERS analysis (Bell and Sirimuthu, 2008; Meng et al., 2018; Zhang et al., 2015b). The ratiometric SERS strategy for the detection of miRNA is rare (He et al., 2019) and more ratiometric concepts may contribute to improve the above-mentioned problems. Based on these situations, we try to develop a ratiometric SERS assay for reliable, sensitive, and selective detection of miRNA, which can correct the variations of Raman signal to improve the accuracy and credibility. Traditional ratiometric SERS strategies always employed two different signal probes to achieve the quantitative detection of targets (Qin et al., 2019; Shi et al., 2017; Si et al., 2018), which could improve the accuracy and reliability of SERS system. Nevertheless, the usage of two probes usually suffered from disadvantages such as time-consuming and complicated labeling procedures, and high-cost of reagents. The internal standard (IS) method was considered as an effective ratiometric strategy for calibrating signal fluctuation originated from the interference of measurement conditions and samples (Shi et al., 2018; Song et al., 2018). Hence, it is attractive to develop an IS-based ratiometric SERS assay for reliably and accurately quantitative determination of miRNA.

Many amplification methods have been proposed to further improve the sensitivity of miRNA detection, including hybridization chain reaction (HCR) (Ge et al., 2014; Zhou et al., 2019a), rolling circle amplification (RCA) (Deng et al., 2014; Lu et al., 2018), nuclease-assisted amplification (Bo et al., 2018; Xiao et al., 2018), and nanomaterial-assisted assays (Azimzadeh et al., 2016; Chand et al., 2018) etc. Although the sensitivity of these methods can be significantly improved, they still have many limitations including expensive reagents, poor reproducibility, complicated operation process, and susceptible to reaction conditions etc. Recently, catalytic hairpin assembly (CHA) amplification was considered as a robust signal amplification strategy with enzyme-free and simple isothermal DNA reaction. Moreover, CHA amplification could achieve hundreds-fold catalytic amplification and overcame the limitation of enzymatic amplification including specific reaction conditions, complex operation, and the reaction time dependent on enzyme activity etc. (Quan et al., 2015; Tang et al., 2018; Zhu et al., 2019). However, the non-specific CHA products in the absence of target usually results in a great background noise, which limits the amplification efficiency to some extent. Ellington et al. (Jiang et al., 2013b, 2014) first introduced the mismatched base pairs into the active breathing site of the assembly hairpin probe 2 (H2), which could improve the signal-to-background ratio.

In this work, a novel ratiometric SERS platform was developed for sensitive and reproducible detection of miRNA-21 by coupling an IS sensing strategy with the mismatched CHA amplification for the first time. The Ag nanoparticles-decorated silicon wafer (AgNPs@Si) was fabricated as SERS substrate, with modification of 4-aminothiophenol (4-ATP, served as an IS) on the surface via Ag–S bonds for reliably quantitative detection. Thiolated capture DNA probes containing the sequence complementary to 3' of hairpin probe 1 (H1) were immobilized on the surface of AgNPs by Ag–S bonds. In the presence of target miRNA-21, the CHA amplification could be initiated to form the H1-miRNA-21 intermediate, and then catalyzed the dynamic assembly of H1 and H2 to produce R6G-labeled H1–H2 complexes accompanying with the release of miRNA-21. The released target miRNA-21 could further trigger next cycle, promoting the CHA recycling assembly. Subsequently, the R6G-labeled H1–H2 complexes were captured by the capture DNA binding on the SERS substrate, which remarkably reduced the distance between R6G Raman labels and the surface of SERS substrate, producing strong R6G SERS signal. As a result, with the increase of target miRNA concentration, the Raman intensity from R6G label increased, whereas that from IS remained relatively unchanged, allowing reliably and accurately quantitative detection of different levels of target miRNA based on the ratiometric peak intensity of R6G label and IS. On the basic of mismatched CHA signal amplification and ratiometric strategy, a robust SERS platform was proposed for miRNA determination with desirable sensitivity, selectivity, and reproducibility, showing a great potential in medical research and early clinical diagnosis.

2. Materials and methods

2.1. Chemicals and reagents

Tris-(2-carboxyethyl) phosphine hydrochloride (TCEP), silver nitrate, hydrogen peroxide (H_2O_2, ≥30%), hydrofluoric acid (HF, ≥ 40%), sulphuric acid (H_2SO_4, 98%), 4-aminothiophenol were purchased from Sinopharm Chemical Reagent Co., Ltd. (Shanghai, China). All these reagents were used without further purification. Phosphate-doped (p-type) silicon wafers (100, 0.01–0.05 Ω sensitivity) were obtained from Hefei Kejing Material Technology Co., Ltd. (Hefei, China). All DNA oligonucleotides and miRNAs were synthesized and purified by Takara Biotechnology Co. Ltd. (Dalian, China) and their sequences are shown in Table S1. All miRNAs were diluted in DEPC-treated water to appropriate concentrations to protect from RNase degradation. The TE buffer (10 mM Tris-HCl, 1 mM EDTA, pH 8.0), hybridization buffer (TNaK buffer, 20 mM Tris, 140 mM NaCl, 40 mM $Mg(Cl)_2$, 5.0 mM KCl, pH 7.5), DEPC-treated water, DNA Marker (25–500 bp), 5 × TBE buffer (225 mM Tris-Boric acid, 50 mM EDTA, pH 8.0), and agarose were bought from Sangon Biotech Co., Ltd. (Shanghai, China). RNase inhibitor was obtained from Takara Biotechnology Co. Ltd. (Dalian, China). All solutions used in the experiment were prepared with ultrapure water (≥18.2 MΩ cm, Milli-Q, Millipore).

2.2. Apparatus

The gel electrophoresis was conducted on an electrophoresis apparatus (Tanon EPS 300, China) and imaged on a gel imaging analysis system (Tanon 1600, China). The characterization of the as-prepared SERS substrate was performed by a scanning electron microscopy (SEM) (Zeiss GeminiSEM 300), and an atomic force microscopy (AFM) (NaNoManVs). SERS spectra were collected using an EZRaman-M portable Raman spectrometer with 785 nm excitation wavelength He–Ne laser (Enwave Optronics, Inc.).

2.3. Fabrication of the IS decorated AgNPs@Si chip

The AgNPs@Si SERS substrate was fabricated via *in-situ* growth of AgNPs on a silicon wafer through an established HF-etching method. The silicon wafer was first cleaned according to the reported method (Chen et al., 2017; Wei et al., 2018). Afterwards, the cleaned silicon wafer (0.5 × 0.5 cm) was further immersed into 5% HF solution for 20 min to obtain H-terminated silicon wafer covered by Si–H bonds. Subsequently, the modified chip was immediately submerged into $AgNO_3$ solution containing 10% HF for 5 min, making AgNPs *in-situ* grow on the surface of silicon wafer through reduction reaction and produce AgNPs-decorated silicon wafer (AgNPs@Si). The obtained AgNPs@Si substrate was washed with ultrapure water for three times and then the internal standard (IS) signal molecule of 4-ATP (0.5 μM) was immobilized on the surface of AgNPs via Ag–S bond by incubation for 1 h (IS-AgNPs@Si). The unbounded 4-ATP molecules were removed by washing with deionized water for three times, and the IS-AgNPs@Si chip was dried with a gentle flow of nitrogen.

2.4. Preparation of ratiometric SERS platform based on mismatched CHA signal amplification

The thiolated-capture DNA was first mixed with 5.0 mM TCEP in 10 mM Tris, pH 8.0 and incubated at room temperature for 1 h. The as-prepared IS-AgNPs@Si chip was immersed in the DNA assembly buffer containing 1 μM capture DNA (10 mM phosphate, pH 7.0) for 24 h at room temperature to conjugate the capture DNA. Afterwards, the chip was then treated with phosphate buffer containing 0.1 M NaCl for 14 h to ensure adequate self-assembly between thiolated-capture DNA and AgNPs. Then, the treated chip was fully washed with 100 mM PBS buffer to remove excess DNA and then dried with nitrogen for further measurement.

The CHA amplification system included two hairpin probes (H1 and mismatched H2), TNak buffer, RNase inhibitor, DEPC-treated water and different concentrations of miRNA. The final concentration of RNase inhibitor reached 1 U. μL^{-1}. After amplification for 90 min, the products were injected to the IS-AgNPs@Si chip and hybridized with the capture DNA immobilized on the chip for 30 min at room temperature.

2.5. SERS measurements of target miRNA

SERS measurement was carried out on an EZRaman-M portable Raman spectrometer with 785 nm excitation wavelength He–Ne laser at 25 °C. The acquisition time was 1 s with 3 rounds of accumulation. All Raman spectra in this study were calibrated by the EZRaman-M Raman software with Auto Base Line. Each sample measurement was conducted at least for three times. Other several miRNAs were also measured as the same experimental conditions as target miRNA detection.

2.6. Gel electrophoresis analysis

To demonstrate the feasibility of CHA signal amplification, the sequences of DNA and products of the CHA reaction were analyzed by 5% agarose gel in 1 × TBE buffer at 140 V constant voltage for 20 min. The gels were visualized via Tanon 1600 gel image analysis system.

3. Results and discussion

3.1. Principle of SERS sensor

As we all known, colloidal Au/Ag NP-based SERS-active substrate, which the SERS signal is obtained from the random aggregation of free Au/Ag NPs, especially in the liquid phase, inevitably resulting in poorly reproducible and relatively unreliable SERS signals (Li et al., 2010). Comparing to free Au/Ag NP-based SERS substrates, silicon-based SERS substrates including metallic nanoparticle-decorated silicon wafers, or silicon nanowire arrays, simultaneously feature good uniformity, strong SERS enhancement, superior sensitivity, and adaptable reproducibility (Lin et al., 2017; Wang et al., 2016). Therefore, the AgNPs@Si was fabricated as SERS-active substrate for constructing ratiometric SERS biosensor. The principle of the mismatched CHA amplification coupling with IS-based ratiometric SERS biosensor for sensitive and reliable detection of miRNA-21 is illustrated in Scheme 1. As shown in Scheme 1a, the IS molecules are first immobilized on the AgNPs@Si surface via Ag–S bonds, and then the thiolated-capture DNA is linked on the surface of SERS substrate through Ag–S bond, which is called as AgNPs@Si chip. The H1 and mismatched H2 are primarily treated with annealing process for obtaining complete hairpin structures. As illustrated in Scheme 1b, in the presence of target miRNA-21, the 3′-R6G labeled H1 hybridizes with target miRNA-21 partly to form dsDNA, which makes the H1 unfold and the complementary sequence of H1 to another hairpin DNA H2 expose. Subsequently, the exposed sequence of H1 hybridizes with mismatched H2 to form H1–H2 complexes and the target miRNA-21 is released. More importantly, the liberated target miRNA-21 is available for the next amplification circulation and can unfold another H1 to initiate the assembly of H1 and H2 via CHA reaction, resulting in forming many H1–H2 duplexes. In addition, as shown in Scheme 1c, the R6G-labeled H1–H2 duplexes are captured by capture DNA probes on the SERS substrate (the whole detection system is called as SERS biosensor), which makes the Raman reporter R6G close to the SERS substrate and the characteristic Raman signals of R6G (e.g., Raman peaks at 1364 cm^{-1} and 1509 cm^{-1}) generate, thus the SERS intensity of R6G is strongly enhanced induced by the Ag NP plasmon resonance and the silicon-assisted plasmon resonance. Meanwhile, the Raman signal intensity of 4-ATP at 1079 cm^{-1} remains relatively constant during this conversion process.

In this experiment, the signal of 4-ATP at 1079 cm^{-1} serves as an ideal IS which can correct the fluctuations and achieve accurately quantitative analysis, since: 1) the non-specific absorption of other interfering materials can be effectively impeded when the surface of AgNP is covered by a great quantity of 4-ATP molecules; 2) comparing to the intensity of R6G, the 4-ATP locates in a non-interfering region and provides an obvious response. Therefore, 4-ATP is expected to serve as an ideal IS, realizing the reliably quantitative detection of target miRNA-21 based on the SERS relative intensities ($I_R = I_{1364}/I_{1079}$). As a result, the value of I_R continually increases with the increase of miRNA-21 concentration. To the best of our knowledge, it is the first report of ratiometric SERS biosensor based on mismatched CHA amplification for the determination of miRNA.

3.2. Characterization of the AgNPs@Si chip

The morphology of the as-prepared AgNPs@Si chip was characterized by scanning electronic microscopy (SEM) and atomic force microscopy (AFM). First, SEM images of the AgNPs@Si chip prepared with different concentrations of silver nitrate ($AgNO_3$) are shown in Fig. 1(A-E). It indicates that the AgNPs are prepared with different sizes and morphology under different concentrations of $AgNO_3$. The average sizes of AgNPs were calculated to be ~60, ~90, ~110, ~130, and ~140 nm for the AgNPs@Si prepared with $AgNO_3$ concentrations of 1, 2, 3, 4, and 5 mM, obtained by the random measurement of 300 AgNPs in the corresponding SEM images. Specially, in the case of $AgNO_3$ concentrations lower than 2 mM, homogeneous nanoparticles with smaller sizes about ~60–90 nm are obtained (Fig. 1A and B). When the $AgNO_3$ concentration gradually increases, AgNPs become larger (~110–140 nm, Fig. 1C–E). These results indicate that the AgNPs prepared with 3 mM $AgNO_3$ are distributed uniformly on the surface of silicon wafer, signed as 3-AgNPs@Si. Moreover, it concludes that the 3-AgNPs@Si SERS substrate includes Si and Ag element, which is confirmed by the EDX spectroscopy (Fig. 1G). The Si peak originates from the silicon wafer, while the Ag peak is assigned to the element from AgNPs. The result of EDX spectroscopy indicates that the 3-AgNPs@Si chip contains Si and Ag in different ratios: ~17.11% Ag in weight ratio and ~4.32% Ag in atomic ratio. Then, SERS measurements of different AgNPs@Si chips are carried out using 4-ATP as the probe. As illustrated in Fig. 1H, the Raman intensity of 4-ATP on the 3-AgNPs@Si is the maximum, demonstrating that the prepared 3-AgNPs@Si is the best SERS chip. Next, to investigate the reproducibility of 3-AgNPs@Si chip, SERS mapping spectra of 4-ATP were obtained by collecting from 50 random spots on the surface of AgNPs@Si substrate (Fig. S1). The result demonstrates that the spectra of 4-ATP are almost identical of 3-AgNPs@Si chip with a small relative standard deviation (RSD) value of ~15.1% (Raman intensity of 4-ATP at 1079 cm^{-1}), suggesting the robust uniformity and reproducibility of Raman signals on the obtained 3-AgNPs@Si chip. The prominent reproducibility of the SERS substrate is attributed to the *in-situ* deposition of AgNPs on the silicon wafer, which can tightly immobilize nanoparticles on the surface and effectively prevent them from random aggregation.

Subsequently, the SERS performance of 3-AgNPs@Si chip was investigated. As shown in Fig. S2, the AgNPs@Si chip produces strong Raman signal as high as ~13 000 after modification of 10 mM 4-ATP,

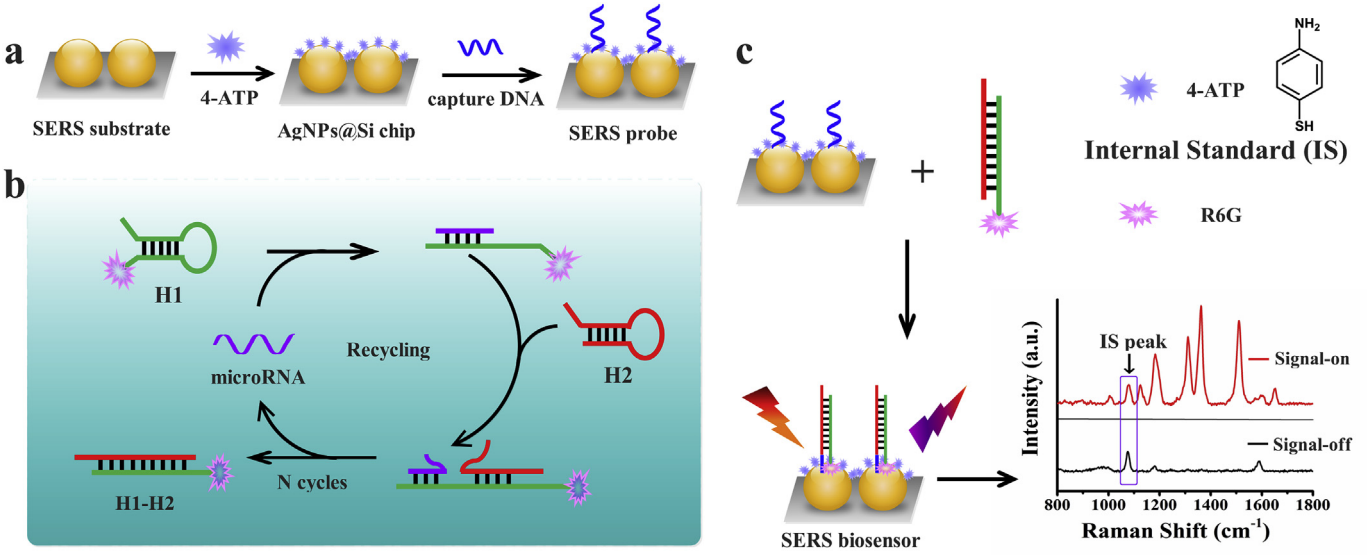

Scheme 1. Schematic of the ratiometric SERS platform based on mismatched CHA amplification for quantitative detection of miRNA-21. (a) Fabrication of the IS-AgNPs@Si SERS probe. (b) The miRNA-induced mismatched CHA amplification process. (c) The principle of ratiometric SERS biosensor for miRNA-21 detection.

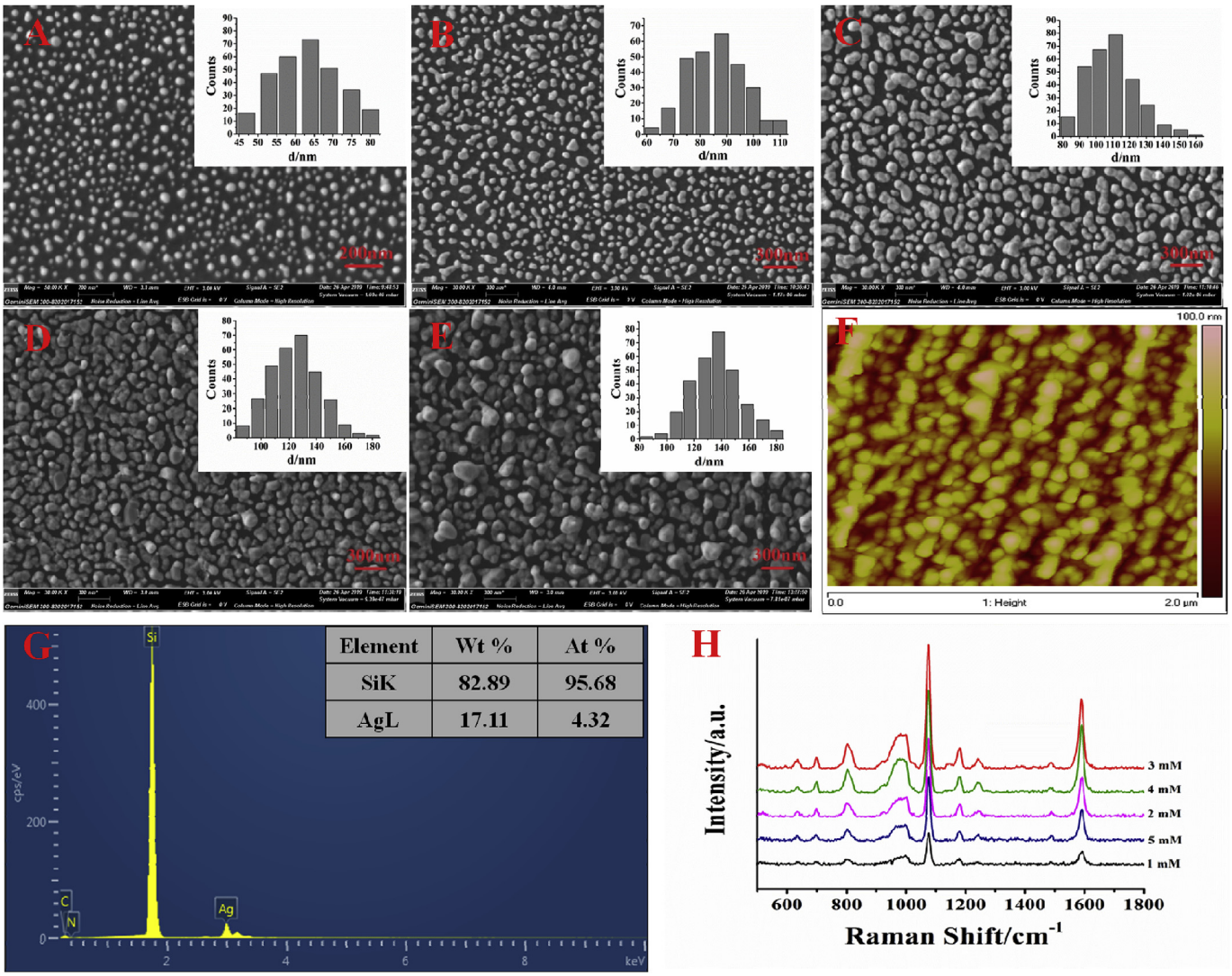

Fig. 1. SEM images of AgNPs@Si chips prepared with different concentrations of $AgNO_3$: (A) 1 mM, (B) 2 mM, (C) 3 mM, (D) 4 mM, (E) 5 mM. (F) AFM image of the as-prepared AgNPs@Si chip with 3 mM $AgNO_3$ (3-AgNPs@Si chip). (G) The elemental ratio of 3-AgNPs@Si chip calculated by EDX spectroscopy. (H) SERS spectra of 10^{-5} M 4-ATP dispersed on the surface of different AgNPs@Si chips.

while Raman signal intensity of 4-ATP dispersed on the naked silicon wafer without AgNPs disposition is much weaker under the same experimental conditions. The SERS enhancement factor (EF) of as-prepared AgNPs@Si SERS substrates are estimated to be $\sim 8.9 \times 10^5$, 1.5×10^6, 2.1×10^6, 1.8×10^6, and 1.1×10^6 for the AgNPs@Si obtained with different $AgNO_3$ concentrations of 1, 2, 3, 4, and 5 mM and the detail calculation of EF is presented in Supporting Information. It can be concluded the EF increases with the size of AgNPs and reaches maximum when the AgNPs is ~110 nm. With the increase of $AgNO_3$ concentration, the nanoparticles aggregate and become inhomogenously, which results in the decrease of EF. It is worthwhile to point out that appropriate aggregation is benefit to create of "hot spots" and enhancement of SERS signals, while severe aggregation is detrimental to reproducibility and enhancement of SERS (Jiang et al., 2013a; Wei et al., 2013). This giant SERS enhancement may be from the boiling electromagnetic field in hot spots that are produced by the effectively coupled between AgNP itself and interconnected AgNPs with the semiconducting silicon wafer (Peng et al., 2010).

3.3. Design and validity of the mismatched CHA amplification system

In the mismatched CHA system, two component DNA hairpins (H1 and H2) were first analyzed by Oligo Analyzer 3.1 to predict their conformations and other parameters (Fig. S3). The parameters are ΔG (gibbs free energy), ΔS (entropy change), and ΔH (enthalpy change) respectively. ΔH is used to identify that the reaction is exothermic or endothermic. According to the Gibbs−Helmholtz (G-H) equation: $\Delta G = \Delta H - T\Delta S$, the values of parameters including ΔG, ΔS, and ΔH are lower, the hairpin structure designed in this experiment is more stable and has rarely other secondary structure, which is beneficial for CHA reaction to decrease the generation of large background signal (Datta and LiCata, 2003; Li et al., 2016). According to the above-mentioned principle and the sequence of miRNA-21, H1 and H2 are designed and their structures are exhibited in Fig. S3. As shown in Fig. S3, the melting temperature of H1 and H2 are 78.3 °C, and 75.2 °C respectively, which are much higher than the reaction temperature (37 °C).

To further verify the CHA reaction, the products and sequences of CHA reaction are featured using 5% agarose gel. As shown in Fig. 2, H1 and H2 maintain stable in the absence of target miRNA-21 (Lane 5), indicating that the cross-reaction between H1 and H2 is negligible. The target miRNA-21 can successfully unfold H1 in the absences of H2 (Lane 6). Upon addition of miRNA-21, a mixture of H1 and H2 appears a new band (Lane 7), which coincides with that of annealed H1 and H2 product (Lane 8), suggesting the successful CHA reaction.

3.4. Optimization of experimental conditions

The performance of this ratiometric SERS platform can be potentially influenced by the number of mismatched bases of H2, the concentration ratio of H1 and H2, the CHA incubating time, and the CHA incubating temperature. Different analytical conditions were investigated in this work. First, two hairpin probes (H1 and H2) in the CHA amplification can possibly react non-specifically despite in the absence of target, which decreases the signal-to-noise ratio (S/N). According to the previous reports, the mismatched bases were executed at the 3′ termini of H2 to reduce the background noise (Zhang et al., 2015c). As shown in Fig. S4, the value of S/N increases with the increase of mismatched base number of H2 up to 2, but the value of S/N decreases with further increase of mismatched number. The reason is that appropriate mismatched number of H2 in CHA system can reduce the non-specific products, but excess mismatched number can interfere in the CHA reaction. Therefore, double mismatched bases of H2 is chosen in the following experiments. Second, the concentration ratio of H1 and H2 is optimized. As shown in Fig. S5, the maximum value of SERS relative intensities ($I_R = I_{1364}/I_{1079}$) is achieved at 1:1, indicating that 1:1 is the optimal concentration ratio of H1 and H2. In addition, the effect of CHA incubating time is also investigated in Fig. S6. The value of I_R ascends with the increase of incubating time. While the incubating time extends to 90 min, the value of I_R shows a stable trend. Therefore, 90 min is chosen as the optimal incubating time for CHA amplification. Temperature is an important parameter of reaction kinetics and determines the probability of collision between the molecules. In this experiment, incubating temperature is a critical factor that influences the stability and interaction of hairpins. The H1 and H2 can not obtain an adequate probability of collision that greatly decreased the formation of H1–H2 duplexes at low temperature. On the contrary, the specificity of this platform will be diminished by high incubating temperature because the stability and integrality of hairpin probes are related to temperature. In this work, experiments were conducted at temperature ranging from 25 to 50 °C for optimization of the incubating temperature. Experimental date is exhibited in Fig. S7 and the result indicates that the value of I_R reaches a peak value at 37 °C, suggesting that 37 °C is the optimum incubating temperature.

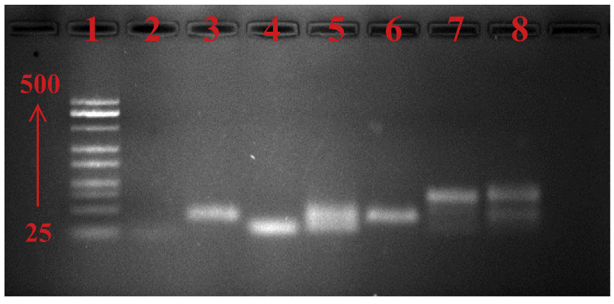

Fig. 2. Gel electrophoresis of CHA amplification products using 5% agarose gel. Lanes 1–8: DNA marker, miRNA-21, H1, H2, H1 + H2, H1 + miRNA-21, H1 + H2 + miRNA-21, H1 + H2 after annealing (the mixture was heated to 95 °C for 10 min and gradually cooled to room temperature). The final concentration of DNA was 1.0 μM.

3.5. Determination of miRNA-21

Under the optimal experimental conditions, this proposed ratiometric SERS platform was used to analyze different concentrations of target miRNA. On one hand, a poor linearity between the logarithmic concentration of miRNA-21 is obtained without correction by the SERS signal of 4-ATP. The corresponding linear fitting with a low linear correlation coefficient (R^2) of 0.972 is displayed in Fig. S8. On the contrary, with the increase of miRNA-21 concentration, the intensity of the peak at 1364 cm^{-1} increases correspondingly, while the peak at 1079 cm^{-1} remains relatively unchanged (Fig. 3A), which causes the ratiometric relative peak intensities I_R to increase accordingly. As a result, a good linearity between the logarithmic concentration of miRNA-21 ranging from 10 fM to 100 nM with a R^2 of 0.994 and the normalized SERS intensity of R6G at 1364 cm^{-1} corrected by the SERS intensity of 4-ATP at 1079 cm^{-1} is obtained as shown in Fig. 3B. The result demonstrates 4-ATP is an ideal IS, which significantly improves the accurately quantitative ability of the SERS sensor for the determination of target miRNA. The limit of detection (LOD) is estimated to be 3.5 fM (S/N = 3) and the detail of LOD calculation method is listed in the Supporting Information. It reveals that this developed platform is efficient for reliably quantitative and sensitive detection of miRNA-21, which is attributed to the employment of mismatched CHA amplification and ratiometric SERS strategy. A comparison with other CHA-based strategies for the detection of miRNA using different techniques are shown in Table S2. Compared to most of other CHA-based methods, the ratiometric SERS-based biosensor proposed in our work has a comparatively lower or at least a similar detection limit. More importantly, this developed method avoids sophisticated instrument, providing an on-site, sensitive, and reliable approach for miRNA

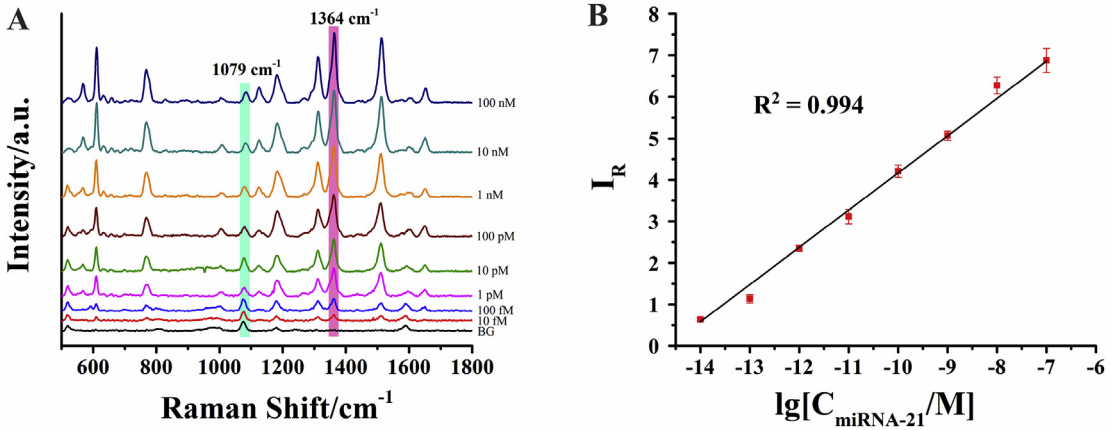

Fig. 3. Ratiometric SERS assay performance for miRNA-21 detection. (A) SERS spectra of the ratiometric biosensor with different miRNA-21 concentrations (10 fM-100 nM). Background (BG) presents for distilled water. (B) The linear fitting of the SERS relative intensities (I_R) *vs.* the logarithmic of miRNA-21 concentrations. Error bars show the standard deviations of three independent assays.

detection with a portable Raman spectrometer.

3.6. Selectivity of the miRNA assay

To further investigate the selectivity of the developed assay, three kinds of interference sequences including miRNA-141, single-base mismatched (SM) and three-base mismatched (TM) miRNA-21 were added into the reaction system, respectively. As shown in Fig. 4A, the spectra include the blank, miRNA-141, SM miRNA-21, TM miRNA-21, target miRNA-21, and their mixtures, suggesting that the SERS signals of miRNA-141, SM miRNA-21, and TM miRNA-21 are similar to that of blank, while remarkable increase in the SERS signal can be found in the presence of target miRNA-21. According to Fig. 4B, the values of I_R of CHA-based SERS biosensor incubated with miRNA-141 or TM miRNA-21 are close to the blank. A slight increase of the I_R value is observed when the biosensor is incubated with SM miRNA-21. However, the target miRNA-21, which the concentration is one hundred times lower than the interference miRNAs, exhibits an obvious increased I_R value, demonstrating that the proposed sensing platform has feature of high selectivity for miRNA-21 over other interference miRNAs.

3.7. Reproducibility

As we all known, the reproducibility of SERS signals is a significant property for SERS sensing strategy. To investigate the reproducibility of the ratiometric SERS biosensor in the determination of miRNA, the RSD values of I_R are calculated to be 2.85% in the detection of 1.0 pM miRNA, which is obtained by collecting from 30 spots in a defined area of 10 × 10 μm^2 of the SERS mapping spectra (Fig. 5A), suggesting the good uniform of the SERS substrate. Moreover, the reliability of the proposed SERS sensor was evaluated via collection from ten different SERS chips under the same experimental conditions (Fig. 5C). As shown in Fig. 5D, the RSD of the values of I_R is 3.73%, which exhibits good reproducibility.

3.8. Stability

Furthermore, the developed biosensor remains available after 30 days storage at 4 °C. Although the intensities of SERS signal have obvious changes, the value of I_{1364}/I_{1079} has no evident change, indicating that the proposed ratiometric SERS biosensor has good stability (Fig. S9). The reason for the good stability of the developed strategy depends mainly on that two Raman labels in the same environment have a similar Raman signal enhancement, consequently, the I_{1364}/I_{1079} value can remain relatively stable.

3.9. Reusability

In addition to the sensitivity, selectivity, and stability of the miRNA SERS biosensor, the reusability is significant in its practical

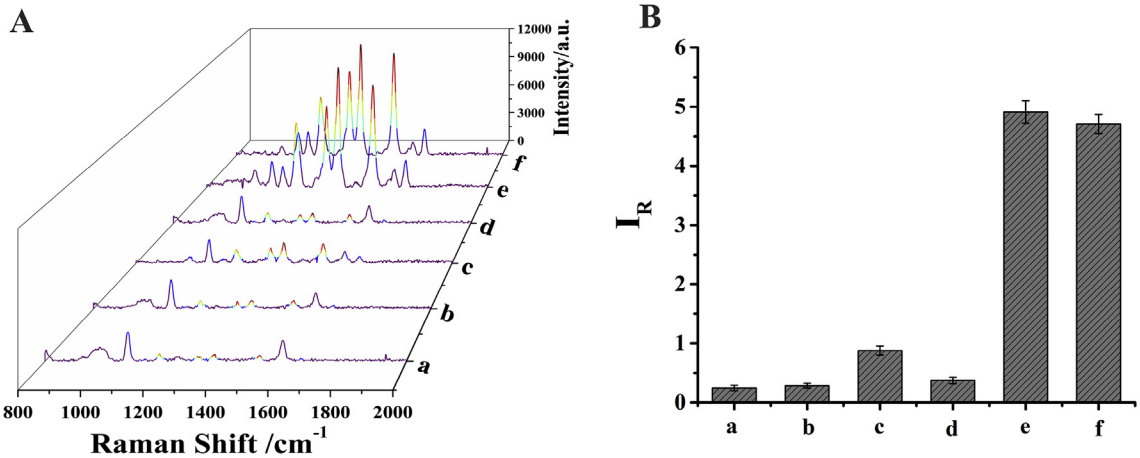

Fig. 4. (A) SERS spectra and (B) the value of I_R (I_{1364}/I_{1079}) respectively responding to (a) blank, (b) miRNA-141, (c) single-base mismatched miRNA-21, (d) three-base mismatched miRNA-21, (e) target miRNA-21, and (f) a mixture of all four miRNAs. Error bar represents the standard deviation of measurement taken from three different experiments. The concentrations of SM miRNA-21, TM miRNA-21, and miRNA-141 are 100 nM, while the concentration of target miRNA-21 is 1.0 nM.

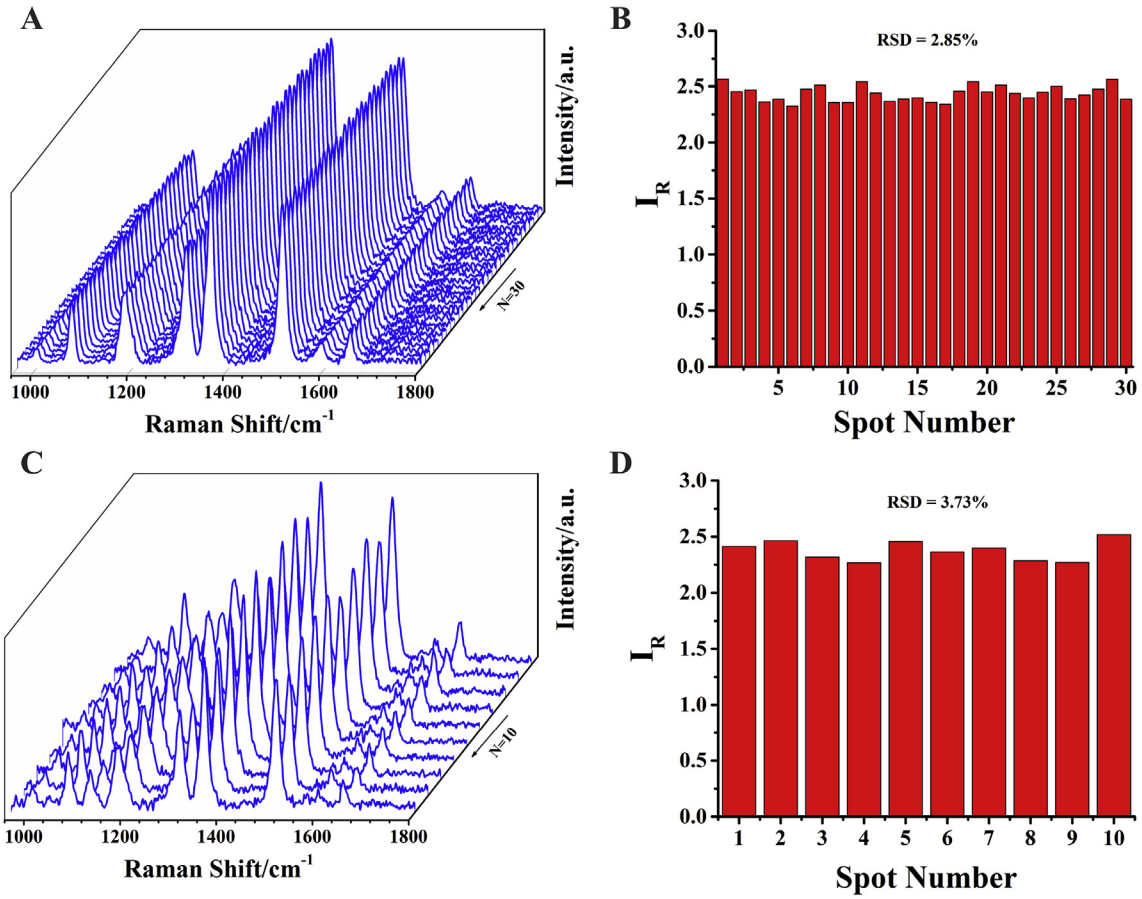

Fig. 5. (A) SERS mapping spectra of the ratiometric SERS biosensor in the detection of 1.0 pM miRNA and (B) corresponding histogram for the value of I_R (I_{1364}/I_{1079}) collected from 30 different spots in a defined area of 10 × 10 μm^2. (C) SERS spectra and (D) histogram for the value of I_R from 10 different SERS substrates.

applications. Fortunately, the developed ratiometric SERS biosensor has a good reusability upon supplementation of target miRNA to forming R6G-labeled H1–H2 complexes. As shown in Fig. S10a, after washing with water once, the washed capture DNA-SERS probe was then applied into another round of detection. Fig. S10b exhibits three-cycles Raman spectra of the ratiometric SERS biosensor in the detection of 1.0 nM miRNA. During each cycle, the Raman intensity of R6G at 1364 cm^{-1} sharply decreased when washed with water, while its intensity readily recovered almost to the initial state after addition of the miRNA-assisted CHA product. The RSD value of the ratiometric SERS signals is 4.1% within three cycles (Fig. S10c), indicating the good reusability of the proposed ratiometric SERS biosensor.

3.10. Biological real sample analysis

The validity of our biosensor was investigated in total RNA extracts from three human cancer cell lines, including the human breast cancer cell lines (MCF-7), mammary epithelial cell lines (MCF-10A), and cervical cancer cell lines (Hela). The relative expression levels of miRNA-21 in those three cell lysate samples were detect using the developed method and the quantitative real-time polymerase chain reaction (qRT-PCR), respectively. The results indicated that the determined relative expression levels of miRNA-21 in the three cell lysates were consistent with those achieved employing qRT-PCR (see Fig. S11 in the Supporting Information). Moreover, these results also revealed that MCF-7 cell lines had higher miRNA-21 expression level than MCF-10A and Hela cell lines, which was in good agreement with previous report (Lu et al., 2005). In addition, different concentrations of miRNA-21, which were spiked into the MCF-10A cell lysates, were also effectively measured by our developed strategy. The experimental dates exhibited in Table S3 show good recovery rates of standard addition from 97.3% to 105.1%. Moreover, to further demonstrate the capacity of the developed biosensor applied in tumor cell extractions analysis, human lung adenocarcinoma cell line (A549) was used to measure the expression of miRNA-21 and the results are shown in Fig. S12A. It is evident that the increasing number of A549 tumor cells (from 10^2 to 10^6) results in a gradual increase in the value of I_R. By plotting the logarithm of the number of A549 cells *vs.* the value of I_R (Fig. S12B), a linear equation of FX (R^2 = 0.994) can be achieved, and the detection limit for the A549 cancer cells is estimated to be 67 cells. These above results demonstrate that this developed sensing platform holds great potential in real biological samples with great accuracy and reliability for the analysis of miRNA-21.

4. Conclusions

In summary, an enzyme-free ratiometric SERS biosensor based on mismatched CHA amplification system has been developed, allowing sensitive, selective, and reliable determination of miRNA. The enzyme-free CHA reaction overcame the defects of traditional enzyme-based amplification and decreased the background signal of CHA system by introducing mismatched base pairs in H2. Furthermore, the IS-based ratiometric strategy with one Raman probe can significantly improve the accuracy and reliability of the SERS biosensor. Taking advantages of the ratiometric SERS probe and mismatched CHA signal amplification, a LOD of 3.5 fM for target miRNA-21 has been achieved with a wide linear range. However, because the developed strategy involves a portable Raman instrument and multiple reactions, the sensitivity may be sacrificed to some extent and longer times are needed. Nonetheless, this method obtains excellent reproducibility and selectivity with the

capability of distinguishing single-base mismatch, which holds great application prospects in disease diagnosis and biosensing. By adjusting the sequences of CHA components, our developed platform may be extended to the determination of various targets and presents a general avenue to propose distinct SERS biosensors for different applications.

CRediT authorship contribution statement

Jinyang Chen: Conceptualization, Funding acquisition, Data curation, Formal analysis, Writing - original draft, Writing - review & editing. **Yan Wu:** Conceptualization, Funding acquisition, Data curation, Formal analysis, Writing - original draft, Writing - review & editing. **Cuicui Fu:** Data curation, Formal analysis, Funding acquisition. **Haiyan Cao:** Methodology. **Xiaoping Tan:** Methodology, Formal analysis. **Wenbing Shi:** Formal analysis, Funding acquisition. **Zhaoyang Wu:** Formal analysis, Writing - review & editing.

Declaration of competing interest

The authors declare that they have no known competing financial interests or personal relationships that could have appeared to influence the work reported in this paper.

Acknowledgements

This research was financially supported by the National Natural Science Foundation of China (No. 21804011 and No. 21705009), the Basic Research Project of Science and Technology Commission of Chongqing (No. cstc2018jcyjAX0721 and No. cstc2018jcyjAX0051), the Municipal Education Commission of Chongqing (No. KJQN201801404), and the Program for Innovation Team Building at Institutions of Higher Education in Chongqing (No. CXTDX201601039).

Appendix A. Supplementary data

Supplementary data to this article can be found online at https://doi.org/10.1016/j.bios.2019.111619.

References

Azimzadeh, M., Rahaie, M., Nasirizadeh, N., Ashtari, K., Naderi-Manesh, H., 2016. Biosens. Bioelectron. 77, 99–106.
Bell, S.E.J., Sirimuthu, N.M.S., 2008. Chem. Soc. Rev. 37, 1012–1024.
Bo, B., Zhang, T., Jiang, Y., Cui, H., Miao, P., 2018. Anal. Chem. 90, 2395–2400.
Boon, R.A., Iekushi, K., Lechner, S., Seeger, T., Fischer, A., Heydt, S., Kaluza, D., Tréguer, K., Carmona, G., Bonauer, A., 2013. Nature 495, 107–110.
Bushati, N., Cohen, S.M., 2007. Annu. Rev. Cell Dev. Biol. 23, 175–205.
Causa, F., Aliberti, A., Cusano, A.M., Battista, E., Netti, P.A., 2015. J. Am. Chem. Soc. 137, 1758–1761.
Chand, R., Ramalingam, S., Neethirajan, S., 2018. Nanoscale 10, 8217–8225.
Chen, N., Ding, P., Shi, Y., Jin, T., Su, Y., Wang, H., He, Y., 2017. Anal. Chem. 89, 5072–5078.
Cialla-May, D., Zheng, X.-S., Weber, K., Popp, J., 2017. Chem. Soc. Rev. 46, 3945–3961.
D'Agata, R., Spoto, G., 2019. Anal. Bioanal. Chem. 411, 4425–4444.
Datta, K., LiCata, V.J., 2003. Nucleis Acids Res 31, 5590–5597.
Deng, R., Tang, L., Tian, Q., Wang, Y., Lin, L., Li, J., 2014. Angew. Chem. Int. Ed. 53, 2389–2393.
Dong, H., Lei, J., Ding, L., Wen, Y., Ju, H., Zhang, X., 2013. Chem. Rev. 113, 6207–6233.
Dong, J., Chen, G., Wang, W., Huang, X., Peng, H., Pu, Q., Du, F., Cui, X., Deng, Y., Tang, Z., 2018. Anal. Chem. 90, 7107–7111.
Driskell, J.D., Seto, A.G., Jones, L.P., Jokela, S., Dluhy, R.A., Zhao, Y.-P., Tripp, R.A., 2008. Biosens. Bioelectron. 24, 917–922.
Ge, Z., Lin, M., Wang, P., Pei, H., Yan, J., Shi, J., Huang, Q., He, D., Fan, C., Zuo, X., 2014. Anal. Chem. 86, 2124–2130.
Guk, K., Hwang, S.G., Lim, J., Son, H., Choi, Y., Huh, Y.-M., Kang, T., Jung, J., Lim, E.-K., 2019. Chem. Commun. 55, 3457–3460.
He, Y., Yang, X., Yuan, R., Chai, Y., 2017. Anal. Chem. 89, 8538–8544.
He, Y., Yang, X., Yuan, R., Chai, Y., 2019. J. Mater. Chem. B 7, 2643–2647.
Jayanthi, V.S., Das, A.B., Saxena, U., 2017. Biosens. Bioelectron. 91, 15–23.
Jeffrey, S.S., 2008. Nat. Biotechnol. 26, 400–401.
Jiang, X.X., Jiang, Z., Xu, T., Su, S., Zhong, Y., Peng, F., Su, Y., He, Y., 2013a. Anal. Chem. 85, 2809–2816.
Jiang, Y., Li, B., Milligan, J.N., Bhadra, S., Ellington, A.D., 2013b. J. Am. Chem. Soc. 135, 7430–7433.
Jiang, Y.S., Bhadra, S., Li, B., Ellington, A.D., 2014. Angew. Chem. Int. Ed. 53, 1845–1848.
Kilic, T., Erdem, A., Ozsoz, M., Carrara, S., 2018. Biosens. Bioelectron. 99, 525–546.
Kosaka, N., Iguchi, H., Ochiya, T., 2010. Cancer Sci. 101, 2087–2092.
Lee, J.U., Kim, W.H., Lee, H.S., Park, K.H., Sim, S.J., 2019. Small 15, 1804968.
Lee, T., Wi, J.-S., Oh, A., Na, H.-K., Lee, J., Lee, K., Lee, T.G., Haam, S., 2018. Nanoscale 10, 3680–3687.
Li, J., Lei, P., Ding, S., Zhang, Y., Yang, J., Cheng, Q., Yan, Y., 2016. Biosens. Bioelectron. 77, 435–441.
Li, W., Camargo, P.H.C., Au, L., Zhang, Q., Rycenga, M., Xia, Y., 2010. Angew. Chem. Int. Ed. 49, 164–168.
Lin, D., Wu, Z., Li, S., Zhan, W., Ma, C., Wang, J., Jiang, Z., Zhong, Z., Zheng, Y., Yang, X., 2017. ACS Nano 11, 1478–1487.
Lu, J., Getz, G., Miska, E.A., Alvarez-Saavedra, E., Lamb, J., Peck, D., Sweet-Cordero, A., Ebert, B.L., Mak, R.H., Ferrando, A.A., 2005. Nature 435, 834–838.
Lu, W., Wang, Y., Song, S., Chen, C., Yao, B., Wang, M., 2018. Analyst 143, 5046–5053.
Masud, M.K., Umer, M., Hossain, M.S.A., Yamauchi, Y., Nguyen, N.-T., Shiddiky, M.J.A., 2019. Trends Biochem. Sci. 44, 433.
Meng, X., Wang, H., Chen, N., Ding, P., Shi, H., Zhai, X., Su, Y., He, Y., 2018. Anal. Chem. 90, 5646–5653.
Mohammadi, H., Yammouri, G., Amine, A., 2019. Curr. Opinion Electrochem. 16, 96–105.
Pang, Y., Wang, C., Lu, L., Wang, C., Sun, Z., Xiao, R., 2019. Biosens. Bioelectron. 130, 204–213.
Peng, Z., Hu, H., Utama, M.I.B., Wong, L.M., Ghosh, K., Chen, R., Wang, S., Shen, Z., Xiong, Q., 2010. Nano Lett. 10, 3940–3947.
Qin, X., Si, Y., Wang, D., Wu, Z., Li, J., Yin, Y., 2019. Anal. Chem. 91, 4529–4536.
Qiu, Z., Shu, J., Tang, D., 2018. Anal. Chem. 90, 1021–1028.
Quan, K., Huang, J., Yang, X., Yang, Y., Ying, L., Wang, H., He, Y., Wang, K., 2015. Chem. Commun. 51, 937–940.
Rafiee-Pour, H.-A., Behpour, M., Keshavarz, M., 2016. Biosens. Bioelectron. 77, 202–207.
Shi, H., Chen, N., Su, Y., Wang, H., He, Y., 2017. Anal. Chem. 89, 10279–10285.
Shi, Y., Chen, N., Su, Y., Wang, H., He, Y., 2018. Nanoscale 10, 4010–4018.
Si, Y., Bai, Y., Qin, X., Li, J., Zhong, W., Xiao, Z., Li, J., Yin, Y., 2018. Anal. Chem. 90, 3898–3905.
Song, Z.-L., Dai, X., Li, M., Song, Z., Chen, Z., Luo, X., 2018. Chem. Commun. 54, 8618–8621.
Su, J., Wang, D., Nörbel, L., Shen, J., Zhao, Z., Dou, Y., Peng, T., Shi, J., Mathur, S., Fan, C., Song, S., 2017. Anal. Chem. 89, 2531–2538.
Tang, S., Gu, Y., Lu, H., Dong, H., Zhang, K., Dai, W., Meng, X., Yang, F., Zhang, X., 2018. Anal. Chim. Acta 1004, 1–9.
Wang, H., Jiang, X., He, Y., 2016. Analyst 141, 5010–5019.
Wei, C., Liu, X., Gao, Y., Wu, Y., Guo, X., Ying, Y., Wen, Y., Yang, H., 2018. Anal. Chem. 90, 11333–11339.
Wei, X., Su, S., Guo, Y., Jiang, X., Zhong, Y., Su, Y., Fan, C., Lee, S.-T., He, Y., 2013. Small 9, 2493–2499.
Wu, H., Liu, Y., Wang, H., Wu, J., Zhu, F., Zou, P., 2016. Biosens. Bioelectron. 81, 303–308.
Xiao, M., Man, T., Zhu, C., Pei, H., Shi, J., Li, L., Qu, X., Shen, X., Li, J., 2018. ACS Appl. Mater. Interfaces 10, 7852–7858.
Zhang, P., Wu, X., Yuan, R., Chai, Y., 2015a. Anal. Chem. 87, 3202–3207.
Zhang, X., Zheng, Y., Liu, X., Lu, W., Dai, J., Lei, D.Y., MacFarlane, D.R., 2015b. Adv. Mater. 27, 1090–1096.
Zhang, Y., Yan, Y., Chen, W., Cheng, W., Li, S., Ding, X., Li, D., Wang, H., Ju, H., Ding, S., 2015c. Biosens. Bioelectron. 68, 343–349.
Zhou, L., Wang, Y., Yang, C., Xu, H., Luo, J., Zhang, W., Tang, X., Yang, S., Fu, W., Chang, K., 2019a. Biosens. Bioelectron. 126, 657–663.
Zhou, M., Teng, C., Li, X., Deng, R., Li, J., 2019b. Anal. Chem. 91, 5295–5302.
Zhou, W., Tian, Y.-F., Yin, B.-C., Ye, B.-C., 2017. Anal. Chem. 89, 6120–6128.
Zhu, H.-Y., Ding, S.-N., 2019. Biosens. Bioelectron. 134, 109–116.
Zhu, M.-H., Mu, X.-M., Deng, H.-M., Zhong, X., Yuan, R., Yuan, Y.-L., 2019. Chem. Commun. 55, 9622–9625.